Journal of Applied Polymer Science

Wireless In-Mold Melt Front Detection for Injection Molding: A Long-Term Evaluation

Florian Müller,[1] Christian Kukla,[2] Thomas Lucyshyn,[1] Matthew Harker,[3] Gerhard Rath,[3] Clemens Holzer[1]

[1]Department of Polymer Engineering and Science, Chair of Polymer Processing, Montanuniversitaet Leoben, Otto Gloeckel-Strasse 2, 8700 Leoben, Austria

[2]Department of Industrial Liaison, Montanuniversitaet Leoben, Peter Tunner Strasse 27, 8700 Leoben, Austria

[3]Department of Product Engineering, Chair of Automation, Montanuniversitaet Leoben, Peter-Tunner-Straße 25, 8700 Leoben, Austria

Correspondence to: F. Müller (florian.mueller@unileoben.ac.at).

ABSTRACT: Wireless sensing technology for injection molding is of increasing interest in literature. Recently, a purely mechanical in-mold sensor for melt front detection was introduced. The sensor system is based on building resonant structures into the mold which are excited by the passing melt front generating structure-borne sound, from which the melt front position is derived. A big advantage of this system is the possibility to implement a plurality of resonant structures while just having one receiver. One important aspect is the need to separate and assign the recorded impinging sounds. A novel algebraic approach was introduced separating the resonant structures by reference to their oscillatory behavior. In this article, measurement results for over 450 injection molding cycles are given proving functionality of the separation process. In addition, it is shown that the melt front detection is reliable and robust when comparing it with results obtained by cavity temperature sensors. © 2014 Wiley Periodicals, Inc. J. Appl. Polym. Sci. **2014**, *131*, 40346.

KEYWORDS: molding; sensors and actuators; thermoplastics

Received 4 October 2013; accepted 22 December 2013
DOI: 10.1002/app.40346

INTRODUCTION

Injection molding is a highly dynamic process for the production of technical parts on a mass production scale. To compensate changing process conditions, that is, batch-to-batch material variation, different control strategies were developed (a comprehensive review of process control is given in.[1] All these strategies rely on sensors obtaining the current state of the process.

For many years, a machine centric approach was used for process control with a focus on high repeatability of the cycles.[2,3] In contrast, the injection mold in series production is often neglected in terms of installing sensors. Groleau[4,5] mentioned that in the year 2002 less than 1% of the injection molding processes in the United States have been instrumented with in-mold sensors. In Germany, it is estimated that solely 5% of the molds are instrumented with in-mold sensors in the year 2011.[6]

However, it would yield large advantages to integrate sensors in the mold for process monitoring and controlling. In Zhang et al.,[7] complex mold modification is listed as a limiting factor to integrate in-mold sensors. In addition, the design hierarchy of a mold plays an important role: first, the desired part geometry is defined, leading to a cooling channel layout enabling a homogeneous surface temperature. Next, ejector pins have to be incorporated to ensure demolding of the part.* With these already fixed parameters, it is often hard to find space inside of a mold to implement the sensors and provide space for the necessary wireducts, especially with the trend of increasing part complexity.[8,9] Furthermore, construction and drilling of wireducts has also a financial impact. In Kazmer,[10] a top-down predictive calculation model for mold construction was presented. It is stated that the costs for the implementation of a sensor† are identical to the implementation of an ejector pin and consequently cannot be neglected. During mold operation and especially during mold maintenance, the sensitive wires have significant disadvantages in terms of being squeezed or ripped off, both cases leading to sensor failure.

*In this example sliders are neglected. With sliders the incorporation of sensors becomes even more difficult.

†Not including the costs of the sensor hardware itself.

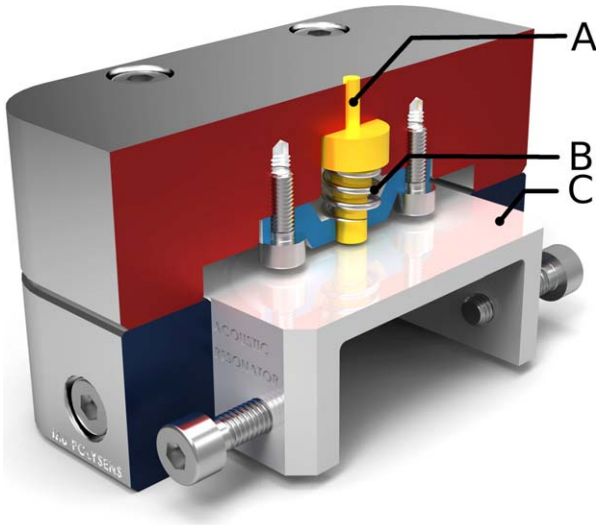

Figure 1. Purely mechanical actuator used to generate a distinctive sound when the melt front passes. The actuator comprises a movable pin (*A*), a supporting spring (*B*), and an exchangeable resonant structure (*C*). [Color figure can be viewed in the online issue, which is available at wileyonlinelibrary.com.]

Currently, two different in-mold sensors are commonly used in injection molding: cavity temperature sensors and cavity pressure sensors.[2] In literature, multiple additional measurement concepts were presented but unfortunately will probably never leave the laboratory state, for example, continuous melt front detection,[11] in-mold fiber orientation sensing,[12] or *in situ* measurements of shrinkage.[13] However, all these sensors are wired.

To eliminate wires inside the mold, a development toward wireless in-mold sensing for injection molding started in the recent years. In 2002, Zhang et al.[9] presented a concept of a wireless self-energized in-mold sensor capable of sensing the melt pressure. Self-energizing of the sensor is essential as currently no energy storage is available to supply the sensors in a 24/7 manner over several months.[14–16] Furthermore, battery storage consumes valuable space within the mold and consequently reduces the advantages of a wireless sensor system. The self-energized sensor converts energy from the melt pressure during injection phase into electrical energy by compressing a piezo stack. The recorded pressure data is transmitted using ultrasonic sound. Ultrasound has the advantage of not being shielded from the metal mass of the mold, which would happen when using radio frequency as the data transmission medium.[17] The sensor concept was developed further to have additional functionality in sensing the melt temperature, too.[18] The research work is still ongoing and is published in a continuous manner, for example, [18–21].

Recently, a mechanical wireless in-mold sensor was introduced, called the acoustic-emission sensor.[22] The sensor is capable of detecting the moment of passing of the melt front and transmits this information using structure-borne sound. The system consists of two main parts, a mechanical actuator implemented in the mold and an accelerometer mounted at an outside surface of the mold to record the structure-borne sound. In Figure 1, a schematic of the mechanical actuator is shown. The actuator comprises an axial movable pin (*A*) protruding approximately 0.5 mm into the cavity chamber. The pin is supported by a spring (*B*) pushing the pin into its initial position. As soon as the melt flows over the pin, the melt pressure acts on the pin accelerating it toward the implemented resonant structure (*C*). On impact, the resonant structure oscillates at its eigenfrequencies. The oscillation is distributed within the metal mass of the mold and can be recorded by the accelerometer mounted on the outside surface of the mold. The increasing melt pressure pushes on the pin aligning it with the cavity surface leading to only a typical ejector mark on the part's surface. The outer dimensions of the acoustic actuator are currently 70 mm length by 50 mm width by 40 mm depth. This setup is larger than essentially necessary to facilitate the exchange of parts. However, a target in future research is the transfer of the acoustic actuator functionality into ejector pins, which are an essential part of an injection mold, that is, Müller et al.[22] Figures 1 and 2. Hence, valuable space near the cavity surface is saved.

Using differently shaped resonant structures, separation of multiple implemented actuators is possible. For the separation, a very efficient linear algebraic approach was introduced recently, called frequency pattern matching algorithm,[23] which is described briefly in this article. In Müller et al.,[24] it was shown that the sensor performance in terms of response time for melt front detection is in comparable range to those of conventional in-mold cavity temperature sensors. In addition, it was shown that the sensor concept is nearly independent of the pressure occurring within the melt in terms of melt front recognition.

The contribution of this article is the investigation of the melt front detection over numerous injection molding cycles, with either one or two mechanical actuators at two different injection flow rates. The capability of the novel algebraic algorithm is investigated to detect the moment of the passing melt front as well as to separate the signals and assign them to the correct resonant structure.

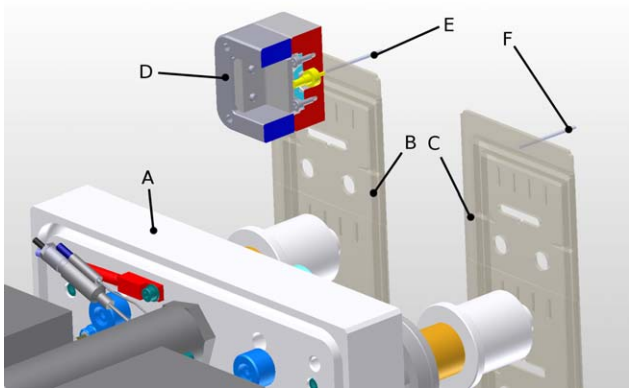

Figure 2. Chosen assemblies of the used test mold are shown as rendered image. The two cavity mold is gated by a symmetrically hot runner (*A*). The two cavities are symmetrical, too, named the left cavity (*B*) and the right cavity (*C*). Only one mechanical actuator is shown located at the left cavity (*D*) with the opposite located cavity temperature sensor (*E*). For the right cavity, the mechanical actuator is not shown but its opposite located cavity temperature sensor (*F*). [Color figure can be viewed in the online issue, which is available at wileyonlinelibrary.com.]

For verification, the received results from the acoustic-emission sensor system were compared to the results obtained by cavity temperature sensors, which are positioned at the same flow path position (but opposite cavity side) and consequently are exposed to the same process conditions as the acoustic-emission sensor system.

EXPERIMENTAL SETUP

For the measurements, a two cavity test mold was used. The chosen assemblies of the mold are shown in Figure 2. The cavities are built symmetrically as well as the hot runner system (*A*). The cavities are labeled as the left cavity (*B*) and the right cavity (*C*) with view direction from the plastification screw. Each nozzle is equipped with an electromechanical valve which can be controlled individually. Both cavities enable the implementation of one mechanical actuator [only shown in the left cavity (*D*)], near the flow path end on the injection side. For verification of the obtained results in terms of moment of passing of the melt front, a cavity temperature sensor (4009b) (*E* and *F*) was placed opposite to each of the movable pins on the ejector side. The cavity temperature sensor 4009b is from Priamus System Technologies AG, Switzerland, with a sensor head diameter of 0.6 mm. It is claimed that the sensor has a response time of 3 ms.[25] With this short response time cavity, temperature sensors are perfectly suited for melt front detection.[26,27] As a result of the sensor position, identical process conditions are present for the two independent measurement systems in terms of melt front detection.

For structure-borne sound recording, the accelerometer 352A60 from PCB Piezotronics, was mounted on an outside surface of the mold. The sensor is capable of detecting frequencies of up to 60 kHz. The measurements were recorded using Data Acquisition System USB-6366 (DAQ) from National Instruments. The accelerometer as well as the cavity temperature sensors and an additional signal from the injection molding machine for process synchronization were recorded synchronously. The DAQ was set to record with a sampling frequency of $f_s = 120$ kHz.

The calculations were performed using MATLAB, from The MathWorks. The calculations were not performed in real time, but were evaluated after the measurements. However, with the used method, the frequency pattern matching algorithm, the number of floating point operations is known *a priori*. Consequently, the approach is by definition suitable for real-time applications.[28,29]

The measurements were performed on an injection molding machine Allrounder 470A 1000-400 alldrive from Arburg, Germany. The material used was a polypropylene C7069 from The Dow Chemical Company, Switzerland. The material is an easy flowing grade having a zero shear viscosity of around 150 Pas at 220°C. Consequently, only low pressure levels are reached during the process. As melt pressure is the driving force for the activation of the actuator, materials with a higher viscosity level will most probably reach even better results than the ones shown. For the measurements performed with two mechanical actuators, an injection flow rate of $\dot{V}_{90} = 90$ cm^{3}s^{-1} was set up. For the measurements with only one mechanical actuator, the injection flow rate was set to $\dot{V}_{60} = 60$ cm^{3}s^{-1}.

For the measurements presented, two differently shaped resonators were used. One is shown in the section view rendering in Figure 1. It is a plate resonator with the outer dimensions of 33 mm length by 28 mm width by 3 mm height. The second resonator, not shown, is a tongue resonator with the same outer dimensions as the plate resonator. For simplicity, both resonators will be referenced by their primary modal frequency. Hence, the plate resonator is referred to as the 12 kHz resonator, and the tongue resonator is referred to as the 3.8 kHz resonator.

SIGNAL PROCESSING

The aim of signal processing is to implement optimal detectors, optimal in terms of noise performance, for the characteristic oscillations of the resonators. Due to the complex mechanical shape and internal reflections within the mold, the signals from the resonators are not fully independent. Consequently, classical correlation detectors[30] will not function optimally.

The usage of structure-borne sound as the data transmitting medium yields challenges especially in the environment of an injection molding machine. The machine itself as well as auxiliary units, such as connected cooling units, produce structure-borne sound exacerbating the signal quality. Hence, the implemented algorithm has to deal with the present situation, that is, suppress spurious noise and amplify the desired information.

In Müller et al.,[23] a new algebraic approach is presented for signature recognition, which is numerically efficient, while maintaining the advantages of full spectrum pattern matching, called the frequency pattern recognition algorithm. In addition to the matching of the pattern, the new method also computes the covariance propagation, which in turn yields a confidence interval. Consequently, the certainty of the measurement is also determined.

The method consists of two steps, signature identification and signature matching. The signature identification can be seen as a calibration step and is performed prior to the measurements. For that the frequency response[‡] s_i of each resonator i is measured. Unfortunately, the resonators' frequency responses are not fully independent to each other. Hence, an orthogonalization process has to be applied which leads to orthogonal signatures $\hat{s}_i$, which form the columns of the signature matrix S. In addition, the signatures are normalized so that S is formed as,

$$S = \left[\frac{\hat{s}_1}{|\hat{s}_1|}, \ldots, \frac{\hat{s}_n}{|\hat{s}_n|} \right] \tag{1}$$

for all n resonators.

During runtime, signature matching is performed yielding a coefficient vector c. Thereby, the ith column of c holds the result for the ith resonator. The coefficient yields the information on how much of the signature is currently present in the recorded measurement signal y. The calculation of c can be denoted as,

[‡]A brief note on nomenclature: matrices are indicated by upright capital letters, e.g. H, and vectors by upright lowercase letters, e.g. y.

$$c = S^{+} F\{I - G_d G_d^T\} y = S^{+} F H y = L y \quad (2)$$

with,

$$H \triangleq \{I - G_d G_d^T\} \quad (3)$$

and

$$L \triangleq S^{+} F H = S^{+} F\{I - G_d G_d^T\}. \quad (4)$$

In eq. (2), S^{+} is the Moore-Penrose pseudoinverse of S,[31] F is the matrix operator of the discrete Fourier transform (DFT), I is the unit matrix, and G_d contains a Gram polynomial basis function set of low degree d.[32] The operator $\cdot^T$ is the transpose of the matrix. Using the projection onto the orthogonal complement, H, of the low degree Gram basis function set G_d will reduce spectral leakage[§] in the spectrum and is consequently an alternative approach to windowing, for example, [33]. Unfortunately, using eq. (2) the temporal component is lost due to the DFT. To preserve a temporal component, the calculation of c is performed similarly to a short-time Fourier transform with a sliding window.

When using the linear operator L for the calculation of the coefficients, it is straightforward to calculate their covariances. When assuming that the noise in the signal y is independent identically distributed (i.i.d.) Gaussian noise with variance σ^2, the covariance matrix Λ_c can be calculated as,

$$\Lambda_c = \sigma^2 L L^T. \quad (5)$$

From the covariance matrix, a confidence interval (e.g., a $3\sigma = 99.73$ %) can be derived estimating the certainty of the calculated coefficients.

RESULTS AND DISCUSSION

Before presenting the results of the long-term measurements, the complete evaluation process is described in detail using one exemplary measurement.

Evaluation Process for Exemplary Result

In Figure 3, a typical measurement result of the recorded structure-borne sound is shown. At the beginning of the injection molding cycle, the opening sound of the electromagnetic valves is recorded which happens at 0.06 and 0.16 s. The temporal difference between the valve opening was selected to enable balanced filling of the two cavities using the method presented in Doppelmayer.[34]

As the total of measurement data per cycle is too large for processing, relevant regions were searched in the signal y. Descriptive statistical methods were used as they are of low computational effort delivering statistical relevant regions. For this purpose, the time varying standard deviation $|\sigma|(t)$ and the time varying skewness $|\mu_3|(t)$ of the recorded signal y are calculated.[35] The area where statistical relevant portions of the signal were searched for are indicated by red solid lines. At 0.7 s, a red solid line indicates the start point and the end point is at 1.5 s. The area is set up with the prior knowledge of the flow path location of the mechanical resonator as well as the

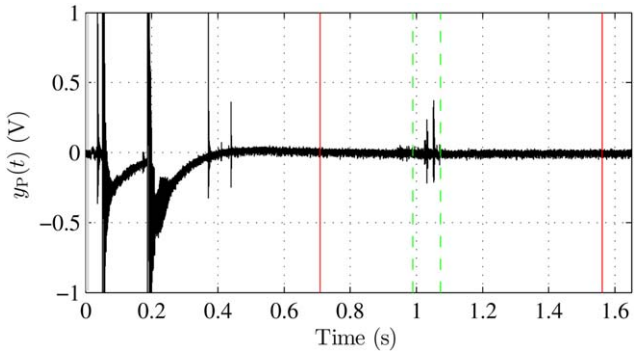

Figure 3. Recorded accelerometer signal y as a function of time. The opening process of both valve gates is realized by electromagnetic actuators resulting in two large deflections ($t_1 = 0.06$ s and $t_2 = 0.16$ s). The opening of the valves is delayed to reduce unbalanced filling of the cavities. In the temporal region confined by the red solid lines, a statistically significant region is sought (identified region is indicated by two green dashed lines) at which frequency pattern matching is performed. [Color figure can be viewed in the online issue, which is available at wileyonlinelibrary.com.]

injection flow rate $\dot{V}$. Using this an expected temporal moment $t_f = V/\dot{V}$, with V the cavity volume needed to reach the mechanical actuator implementation position can be calculated. In the case of the mold used, both cavities have a total volume of $V = 57$ cm^3. Around the temporal moment t_f a search range is defined, indicated by the red solid lines. After finding a point with statistically significant portions, again a temporal range is set, indicated by green dashed lines, at which frequency pattern matching is performed. The reduction of the amount of data in the manner described decreases computation time significantly.

In Figure 4, the result of the coefficient calculation via eq. (2) is shown. In Figure 4, Top the recorded signal y is shown with a temporal focus on the statistically significant region. Two deflections in the signal can be found, one at $t_1 = 0.700$ s and another at $t_2 = 0.715$ s. As only one accelerometer is used which is not directly linked to the resonators, separation is necessary. The target of signal processing is to detect both peaks via the algorithm and assign each of the peaks to the resonant structure which generated the peak.

The two lower plots of Figure 4 show the time varying coefficients c_1 and c_2 as black solid lines. Thereby, coefficient c_1 represents the 12 kHz resonator and c_2 represents the 3.8 kHz resonator.[¶] Both coefficients maintain a low level at the beginning of the time window shown indicating that there is no resonator signature recognized in the signal. They do not stay exactly at 0 which is a result of large levels of noise[**] present in the signal y. At 0.695 s, both coefficient levels rise, whereas c_2 rises significantly higher. This yields the information that the signature of the 3.8 kHz resonator is detected in the signal and consequently the moment of passing melt front in the left cavity. For automatic detection of the moment, a decision process based on statistical methods is used. In case of the first signal

[§]Spectral leakage is the result of aperiodic portions in the signal spreading their energy over the spectrum after applying a DFT and consequently impedes frequency detection.

[¶]This is defined while building up the signature matrix S depending on the column in which the signature of the resonator is stored.

[**]The mounted accelerometer detects a plurality of noise, e.g. connected cooling units and machinery sound.

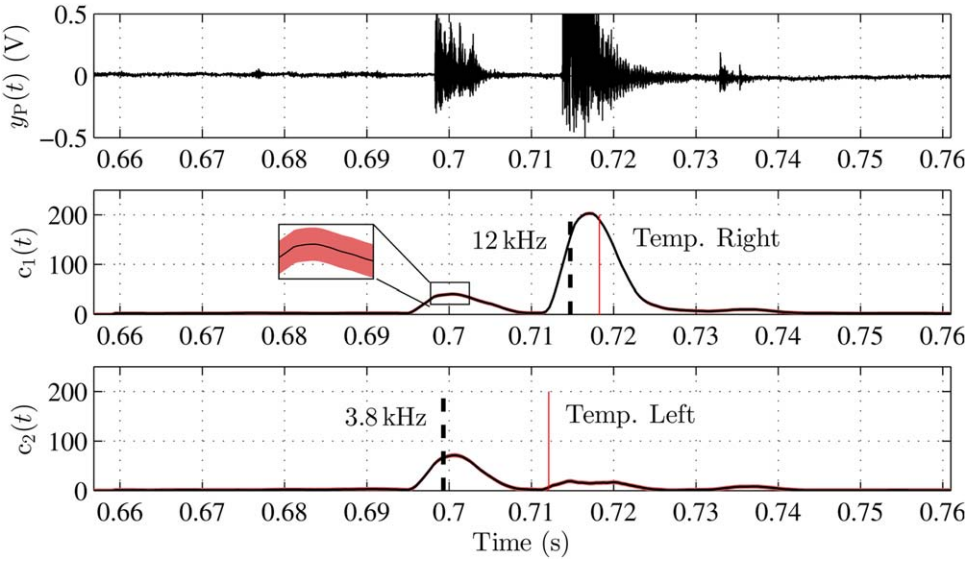

Figure 4. Top: Acoustic signal y with temporal focus on statistically significant region; Middle: Black solid line indicating correlation coefficient c_1 representing the 12 kHz resonator. At around 0.712 s, the correlation coefficient level rises indicating the detection of the 12 kHz resonator (automatic detection indicated by black vertical dashed line). The red vertical line indicates melt front detection via the cavity wall temperature sensor which is implemented in the same cavity; Bottom: Black solid line indicates correlation coefficient c_2 representing the 3.8 kHz resonator. At around 0.695 s, the correlation coefficient level rises indicating the detection of the 3.8 kHz resonator (automatic detection indicated by black vertical dashed line). The red vertical line indicates melt front detection via the cavity wall temperature sensor. The red patch around the correlation coefficients indicates the 3σ confidence interval. [Color figure can be viewed in the online issue, which is available at wileyonlinelibrary.com.]

deflection the 3.8 kHz resonator is detected at 0.699 s. Both coefficients decay back to a level of approximately 0 until the second deflection can be identified in the recorded signal y. Again both coefficients rise, whereby coefficient c_1 increases significantly higher. Using the decision process the 12 kHz resonator is detected at about 0.714 s. From the results obtained, it can be seen that unbalanced filling is present. Unbalanced filling for multicavity molds is addressed in for example, [34, 36].

The following aspects underline the validity of the demonstrated procedure for separation. For both cases, it is true that one of the two peaks inside each coefficient is significantly higher. In addition, when comparing the peaks which occur at the same temporal moment again a reliable differentiation is possible.[††] Furthermore, a red patch indicating the 3σ confidence interval is plotted around each time varying coefficient, giving the certainty of the calculated coefficients. As the confidence interval is very small, a zoomed area of the first peak of the coefficient c_1 is plotted. The 3σ confidence interval for the coefficient c_1 is $\pm$ 4.3 and for the coefficient c_2 it is $\pm$3.6. As a result, separation of the peaks is reliably possible. The difference of the confidence interval size between c_1 and c_2 is a result of measuring the signatures sequentially resulting in different levels of noise. Furthermore, the noise was not evaluated per processing window resulting in one constant value for the confidence interval.

The signals of the cavity temperature sensors can be consulted for the verification of the obtained results. When the hot melt front passes the sensor head, the resulting measurement signal rises sharply enabling the detection of the melt front. As it is a wired sensor, it is easy to say at which position the melt front passed. They are therefore suited for the verification of the obtained results via the acoustic-emission sensor.

For automatic detection of the passing melt front via the temperature sensor, a low-pass filtered signal is subtracted from the recorded signal. This results in a difference signal as a result of filter delay. If the difference exceeds the limit of 1.5°C, the temperature signal increase is detected and consequently this indicates the moment of passing of the melt front.

However, the temperature signals of the two cavity temperature sensors show a different response behavior. In Figure 5, the moment of the passing melt front is shown in detail for both temperature sensors (Figure 5 Middle for the temperature sensor right T_{Right} and Figure 5 Bottom for the temperature sensor left T_{Left}) as well as the acoustic signal y for reference (Figure 5 Top). When comparing the response characteristic at the moment of the passing melt front, one will recognize that T_{Left} has a creeping temperature increase slightly before the temperature signal increases steeply. This can easily be seen when comparing the temperature signal with the black horizontal dashed line which indicates the starting temperature. By interchanging the two temperature sensors, it was shown that this creeping behavior is cavity related and not a sensor malfunction. The final reason is not known, but it is believed that venting is the reason for this issue. As a result, the cavity pressure level rises and leads to an early detection of the melt front via the acoustic-emission system in the left cavity because the air pressure rose and acted on the movable pin. This could have been prevented by either optimizing the venting of the cavity or

[††]Since both coefficients are scaled identically the peaks in c_2 seem to be not so easily differentiable which however is just a result of scaling.

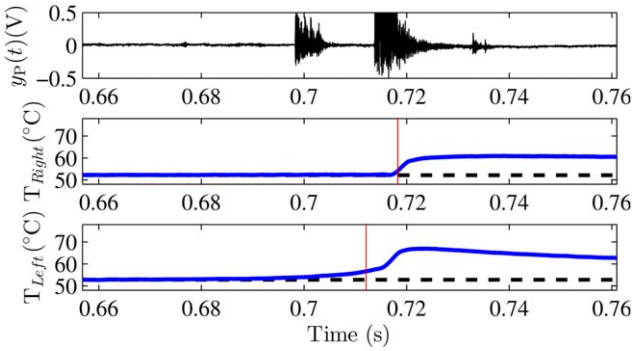

Figure 5. Top: Recorded acoustic signal y with temporal focus on the moment of passing melt front; Middle: Temperature signal T_{Right} indicating the cavity temperature in the right cavity. The red line indicates the calculated moment of passing melt front in the right cavity; Bottom: Temperature signal T_{Left} indicating the cavity temperature in the left cavity. The red line indicates the calculated moment of passing melt front in the left cavity. For both temperature sensors, a black horizontal dashed line indicates the offset temperature for easier recognition of the response characteristic. [Color figure can be viewed in the online issue, which is available at wileyonlinelibrary.com.]

using a stiffer spring to support the movable pin. However, the detection is only shifted by approximately 8 ms and as shall be seen later, this issue does not influence the basic statement of this article and consequently no modification of either the actuator or the cavity has been performed.

Coming back to the melt front detection using the cavity temperature sensors, the detection point is indicated by the vertical red line for each temperature sensor in Figure 4. For the cavity temperature sensor in the right cavity, which is in the same cavity as the 12 kHz resonator (coefficient c_1), the melt front was detected at 0.718 s. For the left cavity temperature sensor in the left cavity, which is in the same cavity as the 3.8 kHz resonator, the passing melt front was recognized at 0.712 s.

For this study, an evaluation criterion for the acoustic-emission sensor is introduced. A difference time between the melt front detection of each system (acoustic and temperature) is calculated. For a total of 257 cycles, this calculation was performed to investigate if the acoustic-emission sensor is capable of detecting the melt front in each cycle at a similar time as the cavity temperature sensor. Consequently, if the acoustic-emission sensor system delivers robust melt front detection the difference time should yield a small standard deviation σ. This in turn would indicate melt front detection at identical instants of time as the cavity temperature sensor. This method has the advantage to compensate the possible occurrence of a temporal shift in the detection of the melt via the two systems.

In case of the example shown, a difference in detection time of $\Delta t_{12\ \text{kHz}} = -3.5$ ms for the 12 kHz resonator and a longer time of $\Delta t_{3.8\ \text{kHz}} = -12.8$ ms for the 3.8 kHz resonator is found. Again, the cavity related issue leads to the fact that the difference time measured for the 3.8 kHz resonator is greater in value. However, this does not affect the statement of this article as the aim of this article is not to compare the two sensor technologies but to use the well established cavity temperature sensors for result verification only.

Long-Term Results for Two Mechanical Actuators

The proposed evaluation method was then applied to all 257 recorded injection molding cycles. Thereby the results are split up in two sections, one dedicated to the cavity related to the 3.8 kHz resonator and one for the 12 kHz resonator. For each resonator different plots are shown, one with difference time over shot number as well as one plot with a histogram of the difference time to estimate the distribution. The goal is to have a narrow standard deviation of the measured difference times, indicating identical functionality from shot to shot. For the 12 kHz resonator additionally a normal distribution plot of the difference time is shown.

In Figure 6, the difference time $\Delta t_{12\ \text{kHz}}$ is plotted. The mean difference time is at $\Delta\bar{t}_{12\ \text{kHz}} = -3.55$ ms and the measurement series has a standard deviation of $\sigma_{12\ \text{kHz}} = 0.28$ ms. The mean value is indicated by a black horizontal line surrounded by a grey patch marking the area of standard deviation. The difference time is negative over all measurements indicating the melt front was recognized by the acoustic-emission sensor in advance of the detection via the cavity temperature sensor.

In Figure 7, the associated histogram plot of the measurement data $\Delta t_{12\ \text{kHz}}$ is shown. The histogram was plotted using bins of 0.11 ms. The difference time is within a small time window of −4.05 to −2.79 ms. Only two aberration values appear, one at −4.5 ms and the second with −5 ms. The reason for these two different values lies in the fact that the detection peak of the coefficient c_1 for these two measurements is slightly smaller in comparison to the majority of the measurements. As the decision process is based on statistics, the moment of detection is slightly shifted leading to a different difference time.

In addition, the histogram data shown in Figure 7 gives the impression that the data is normally distributed. This can be

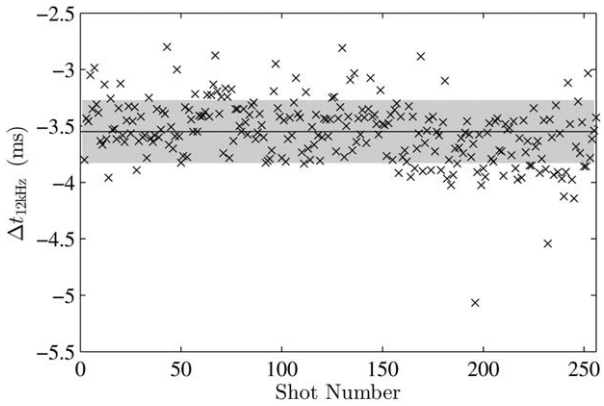

Figure 6. Difference time $\Delta t_{12\ \text{kHz}}$ for a measurement series of 257 cycles comparing detection of 12 kHz resonator with melt front detection via cavity temperature sensor. The mean value over all shots is indicated by a black horizontal line, and the standard deviation of the measurement series is represented with the grey patch around the mean value.

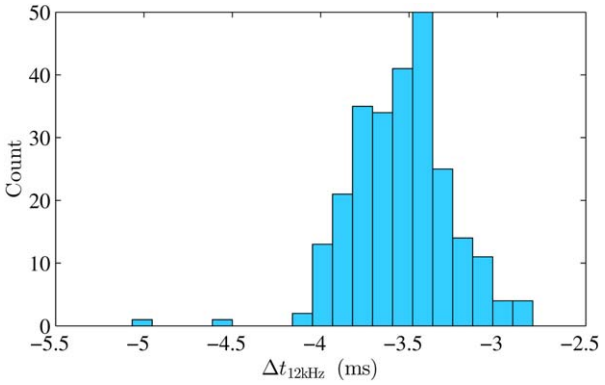

Figure 7. Histogram of the measurement series shown in Figure 6. The bins have a width of 0.11 ms. [Color figure can be viewed in the online issue, which is available at wileyonlinelibrary.com.]

verified using a normal probability plot which is shown in Figure 8.[37] The measurement data follows the fitting line almost perfectly indicating a normal sampling distribution. This in turn shows that the measurement data is symmetrically distributed around the given mean value with the given standard deviation. In addition, the deviation is randomly distributed indicating a typical bias free measurement process.

A similar series of plots is shown for the measurement results for the 3.8 kHz resonator. In Figure 9, the difference time $\Delta t_{3.8\ kHz}$ is shown as a function of shot number. The mean value of the measurement data is at $\Delta\overline{t}_{3.8\ kHz} = -13.70$ ms with a standard deviation of $\sigma_{3.8\ kHz} = 0.78$ ms. The mean value is again indicated by a black solid line, and the standard deviation is marked with the grey patch around the mean value. The measurement series was again investigated toward normal sampling distribution which can be confirmed (no normal probability plot shown). As already discussed, the mean value has an offset resulting from a cavity related issue. The standard deviation obtained is slightly bigger than for the 12 kHz resonator but still rather small for the large amount of measurement data. In addition, a negative slope is recognized from about shot number 120 up to the end of the measurement series. This

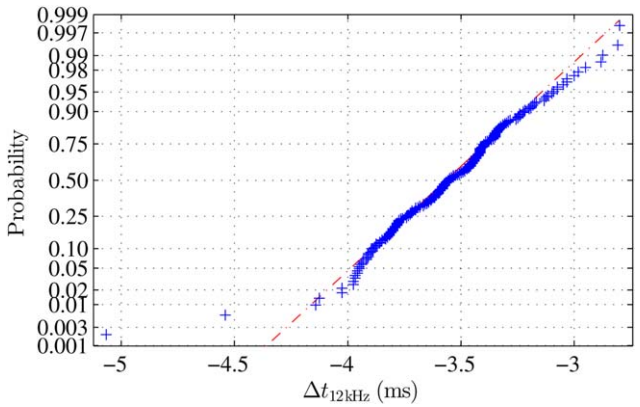

Figure 8. Normal probability plot of the measurement series $\Delta t_{12\ kHz}$. The measurement data follows the fitting line almost perfectly indicating normal sampling distribution. [Color figure can be viewed in the online issue, which is available at wileyonlinelibrary.com.]

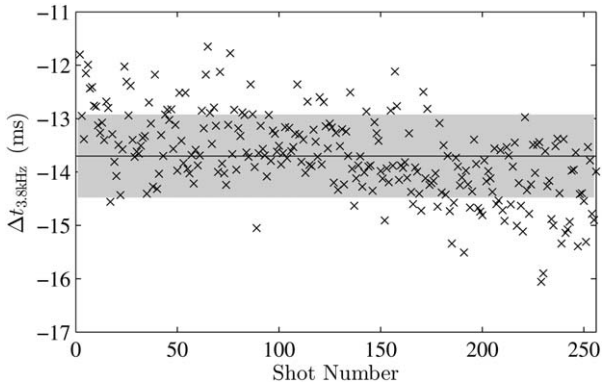

Figure 9. Difference time $\Delta t_{3.8\ kHz}$ for a measurement series of 257 shots comparing detection of the 3.8 kHz resonator with melt front detection via cavity temperature sensor. The mean value over all shots is indicated by a black horizontal line and the standard deviation of the measurement series is represented with the grey patch around the mean value.

indicates that the melt front was even earlier recognized with the acoustic-emission sensor than with the cavity temperature sensor. As no similar trend is found for the 12 kHz resonator (see Figure 6), it is believed that the cavity venting issue is increasing with the shot number. However, the standard deviation was calculated to be small verifying functionality.

In Figure 10, the histogram of the measurement result for $\Delta t_{3.8\ kHz}$ is shown using a bin width of $t_{bin} = 0.21$ ms. The bin width was calculated as,

$$t_{bin} = \frac{|\Delta t_{max} - \Delta t_{min}|}{n}, \tag{6}$$

with n the number of bins, that is, $n=20$ as a practicable value with sufficient resolution.

From the histogram, it can be seen that the measurement data is symmetrically distributed with nearly no aberration values.

To sum this section up, both resonators and in turn the melt front were detected for each of the 257 measurements at constant points of time as it was verified with the cavity temperature sensor indicated by small standard deviation σ. This in turn shows that the measurement concept of the acoustic-

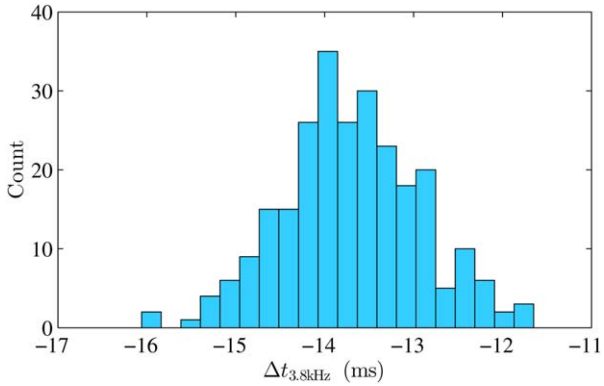

Figure 10. Histogram of the measurement series shown in Figure 9. The bins have a width of 0.21 ms. [Color figure can be viewed in the online issue, which is available at wileyonlinelibrary.com.]

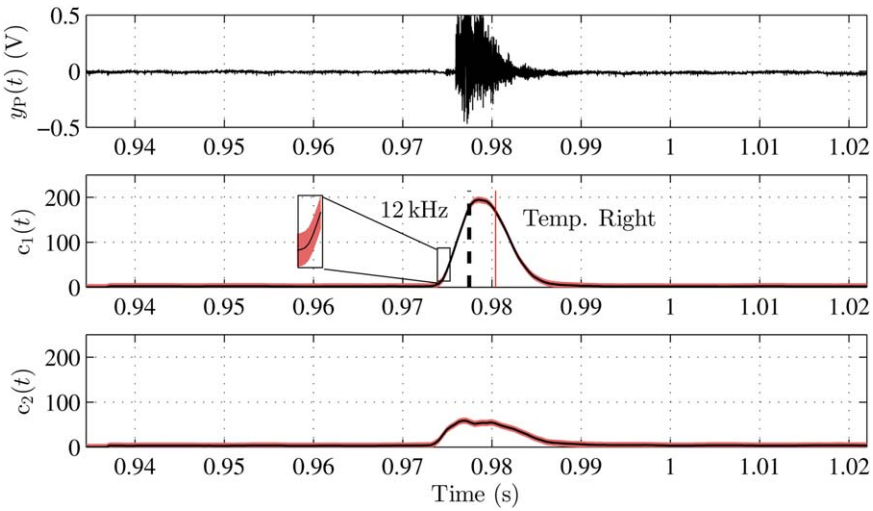

Figure 11. Top: Acoustic signal y in temporal range of pin impact; Middle: Correlation coefficient c_1 representing the 12 kHz resonator. At around 0.975 s, the correlation coefficient level rises indicating the detection of the 12 kHz resonator (automatic detection indicated by vertical black dashed line). The red line indicates melt front detection via the cavity wall temperature sensor; Bottom: Correlation coefficient c_2 representing the not implemented 3.8 kHz resonator for additional verification if separation is possible. Both coefficients have a red patch around the calculated values indicating the 3σ confidence interval. [Color figure can be viewed in the online issue, which is available at wileyonlinelibrary.com.]

emission sensor is capable of detecting the passing melt front over numerous measurement cycles with a very good reproducibility.

Long-Term Results for One Mechanical Actuator

To enhance this statement, additional measurements were performed where one of the resonators was replaced by a blanked insert. For this measurement series, the 3.8 kHz resonator insert was replaced by a blanked insert deactivating the melt front detection in the left cavity. The second cavity stayed untouched, still detecting the melt front using the 12 kHz resonator. The evaluation process stays the same, too, evaluating the coefficients for both resonators. In this manner, separation of the resonators can still be performed verifying if the algorithm works as desired. As a result of the measurement setup, the coefficient for the 12 kHz resonator should stay at a low level over the complete measurement time. For this series, the injection flow rate was changed to $\dot{V}_{60}$=60 cm^3s^{-1} resulting in a detection point at around 1.0 s.

In Figure 11, a sample result is plotted with a temporal focus on the statistically relevant portion of the signal y. In the top plot, the recorded acoustic signal y is shown. In contrast to the measurements with two implemented mechanical resonators, only one large deflection is found in the signal originating from the 12 kHz resonator. Consequently, detection coefficient c_1 should have a significant increase at the temporal moment of the deflection, whereas coefficient c_2 should stay at a low level over the complete measurement period.

The desired situation can be seen in Figure 11 Middle and Bottom. The coefficient c_1 stays at a low level until 0.975 s. It increases significantly enabling the detection of the 12 kHz resonator and consequently detecting the moment of passing of the melt front at 0.977 ms. Afterward, the coefficient decays back to approximately 0. When investigating the behavior of the coefficient c_2, almost the expected trend is observed. Only at the moment of the large deflection in the measurement signal y, the coefficient c_2 rises slightly. Fortunately, the increase is comparably low compared to the increase of coefficient c_1 enabling separation of the two resonators. In addition, when investigating the 3σ confidence interval, which is plotted as a red patch around the time varying coefficient, a reliable separation is obtained.

For verification of the obtained, result the measurement data of the cavity temperature sensor can be used. The signal was evaluated identically as described before. In case of the cycle shown in Figure 11, the melt front was detected at 0.980 s via the implemented cavity temperature sensor. The moment of passing of the melt front recognition is indicated with a red vertical line. For the evaluation of the measurement series, the criterion

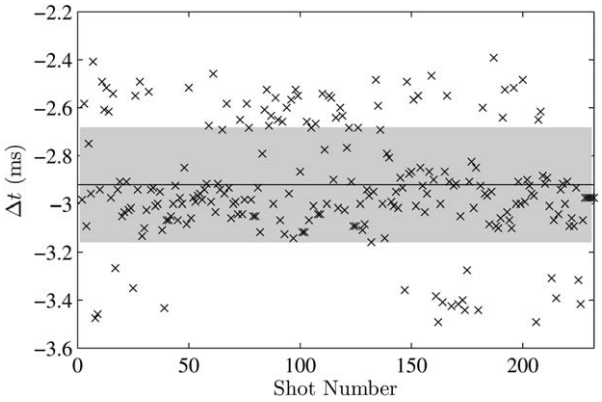

Figure 12. Difference time $\Delta t_{12\ kHz}$ for a measurement series of 225 shots with implemented 12 kHz resonator. The mean value over all shots is indicated by a black horizontal line, and the standard deviation of the measurement series is represented with the grey patch around the mean value.

of difference time is used, measuring the time between the detection of the passing melt front using the two independent systems. In case of the shown measurement, a difference time of $\Delta t_{12\ kHz} = -3$ ms was calculated.

This evaluation process was performed for a total of 225 cycles, calculating the difference time $\Delta t_{12\ kHz}$ over all cycles. The result is shown in Figure 12. The mean value over all shots is at $\Delta \bar{t}_{12\ kHz} = -2.919$ ms shown as a black horizontal line. The standard deviation was calculated as $\sigma_{12\ kHz} = 0.24$ ms indicated by a grey patch. Although the injection flow rate was changed, the difference mean time value and the standard deviation is nearly unaltered in comparison to the measurement results obtained with the injection flow rate of $\dot{V}_{90}$. The standard deviation $\sigma_{12\ kHz}$ is again very low indicating good functionality over all 225 cycles.

To sum up, the melt front was detected for all 225 cycles. Separation was possible as indicated by the coefficient c_2 which stayed comparably low leading to a reliable separation of the resonators. In addition, the difference time value stayed fairly constant over all the cycles indicating that the acoustic-emission sensor is a reliable measurement system.

CONCLUSIONS

In this article, measurement results using the acoustic-emission sensor system were presented. The system is designed for wireless melt front detection inside an injection mold. Using differently shaped mechanical resonators, a distinctive additive sound is generated which can be recorded from an outside surface of the mold. The focus in this article was laid on separating multiple integrated mechanical resonators by their resonance frequency using a novel linear algebraic approach, that is, the frequency pattern recognition algorithm.

For a total number of 482 injection molding cycles, separation was successfully performed. This was verified using conventional in-mold sensing technique, that is, cavity temperature sensors, for comparing the moment of melt front detection via each independent system. For evaluation of the results, a difference time between the melt front detection of each system (acoustic-emission sensor and cavity temperature sensor) was calculated. It was shown that this difference time is stable over the performed injection molding cycles indicating that the novel measurement system delivers reliable results in terms of melt front detection. The calculated standard deviation of the difference time was calculated to be at maximum 0.8 ms which enhances the statement of reliable functionality. Furthermore, it was shown that the difference time is independent from the two different injection flow rates, that is, $\dot{V}_{60}$ and $\dot{V}_{90}$.

OUTLOOK

The main goal is to transfer the sensor technology from the mechanical resonator inserts to ejector pins. This would give ejector pins, which are an essential part of each injection mold, an additional functionality without diminishing their functionality for demolding.

In addition, the time-dependent pin movement is a critical aspect of the sensor system which has not yet been experimentally investigated. This will be done in future research work using a capacitive position sensor recording the pin movement. The resonant structures will be excited identically from shot to shot only if the pin movement is reproducible which in turn will increase the detection reliability. Furthermore, the signature matrix S needs to be improved to reduce cross detection.

A challenging topic that needs to be addressed is real-time signal processing. Only when the recorded signal y is processed online, active machinery control is possible.

Finally, the sensor has to stand a test in a series mold delivering good results over a duration of several tens of thousands of injection molding cycles. This proof, however, cannot be given from tests on a laboratory scale.

ACKNOWLEDGMENTS

The research work was supported by the project "PolyRegion" which is founded by the European Territorial Cooperation SI-AT.

REFERENCES

1. Chen, Z.; Turng, L.-S. *Adv. Polym. Technol.* **2005**, *24*, 165.
2. Giboz, J.; Copponnex, T.; Mélé, P. *J. Micromech. Microeng* **2007**, *17*, 96.
3. Kamal, M. R.; Patterson, W. I.; Fara, D. A.; Haber, A. *Polym. Eng. Sci.* **1984**, *24*, 686.
4. Groleau, R. J. Best Practices with In-Mold Sensors; Society of Plastics Engineering Regional Technical Conference: Erie, **2004**.
5. Kazmer, D. O.; Johnston, S. P.; Gao, R. X.; Fan, Z. *Intern. Polym. Process.* **2011**, *XXVI*, 63.
6. Behrens, H.-H. *Kunststoffberater*, **2012**, 31.
7. Zhang, L.; Theurer, C.; Gao, R. X.; Kazmer, D.O. *IEEE Trans. Ultrason. Ferroelectr. Freq. Control* **2005**, *52*, 1360.
8. Fan, Z.; Gao, R. X.; Kazmer, D. O. Design and Evaluation of a Modulator Circuit for a Self-Energized Wireless Sensor; ASME 2008 International Mechanical Engineering Congress and Exposition, Boston, Massachusetts, USA, October 31–November 6, **2008**
9. Zhang, L.; Theurer, C. B.; Gao, R. X.; Kazmer, D. O. *Trans. North Am. Manuf. Res. Inst.* **2002**, *30*, 573.
10. Kazmer, D. O. Injection Mold Design Engineering; Hanser, Hanser Gardner: Munich, Cincinnati, **2007**.
11. Wang, H.; Cao, B.; Jen, C. K.; Nguyen, K. T.; Viens, M. *Polym. Eng. Sci.* **1997**, *37*, 363.
12. He, B.; Yuan, X.; Yang, H.; Tan, H.; Qian, L.; Zhang, Q.; Fu, Q. *Polymer* **2006**, *47*, 2448.
13. Michaeli, W.; Starke, C. *Polym. Test.* **2005**, *24*, 205.
14. Arshak, K. I.; Morris, D.; Arshak, A.; Korostynska, O.; Jafer, E. *IEEE Sens. J.* **2007**, *7*, 122.
15. Broadbent, H. A.; Ivanov, S. Z.; Fries, D. P. PCB-MEMS Environmental Sensors in the Field; In IEEE International Symposium on Industrial Electronics, Glasgow, Scotland, **2007**.

16. Flammini, A.; Marioli, D.; Sisinni, E.; Taroni, A. *IEEE Trans. Ind. Electron.* **2009**, *56*, 747.
17. Fan, Z.; Gao, R. X.; Kazmer, D. O. Design of a self-energized wireless sensor for simultaneous pressure and temperature measurement; In IEEE International Conference on Advanced Intelligent Mechatronics, Montreal, **2010**.
18. Fan, Z.; Gao, R. X.; Kazmer, D. O., Eds. Self-Energized Acoustic Wireless Sensor for Pressure-Temperature Measurement in Injection Molding Cavity; IEEE Sensors: Christchurch, New Zealand, **2009**.
19. Gao, R. X.; Fan, Z.; Kazmer, D. O. *CIRP Ann.–Manuf. Technol.* **2008**, *57*, 389.
20. Gao, R. X.; Fan, Z.; Kazmer, D. O. US Pat. 2013/0030723 A1, **2012**.
21. Theurer, C.; Zhang, L.; Kazmer, D. O.; Gao, R. X.; Jackson, R. *IEEE Sens. J.* **2006**, *6*, 47.
22. Müller, F.; Rath, G.; Lucyshyn, T.; Kukla, C.; Burgsteiner, M.; Holzer, C. *J. Appl. Polym. Sci.* **2013**, *127*, 4744.
23. Müller, F.; O'Leary, P.; Rath, G.; Kukla, C.; Harker, M.; Lucyshyn, T.; Holzer, C., Eds. Resonant Acoustic Sensor System for the Wireless Monitoring of Injection Moulding; Sensornets 2013: Barcelona, Spain, **2013**.
24. Müller, F.; Kukla, C.; Lucyshyn, T.; Holzer, C., Eds. Performance Evaluation of Purely Mechanical Wireless In-Mould Sensor for Injection Moulding; International Conference on Polymer Engineering: London, UK, **2013**.
25. Priamus System Technologies AG, Datasheet 4009B / 4010B, 2006. Available at: http://priamus.com/english/pdf/Datenblaetter_pdf_e/4009B-e.pdf, accessed on December 5, **2011**.
26. Bader, C.; Zeller, S. C. *Kunstst. Mag. Online* **2010**, 2.
27. Kazmer, D. O.; Velusamy, S.; Westerdale, S.; Johnston, S.; Gao, R. X. *Polym. Eng. Sci.* **2010**, *50*, 2031.
28. Burns, A.; Wellings, A. J. Real-time Systems and Programming Languages: Ada, Real-Time Java and C/Real-Time POSIX, 4th ed.; Addison-Wesley: Harlow, **2009**.
29. Kuo, S. M.; Lee, B. H.; Tian, W. Real-time Digital Signal Processing: Implementations and Applications, 2nd ed.; Wiley: Chichester, England, Hoboken, NJ, **2006**.
30. Fano, R. M. Signal-to-noise Ratio in Correlation Detectors; Massachusetts Institute of Technology, Research Laboratory of Electronics: Cambridge, Massachusetts, **1951**.
31. Golub, G. H.; van Loan, C. F. Matrix Computations, 3rd ed.; Johns Hopkins University Press: Baltimore, **2007**.
32. O'Leary, P.; Harker, M., Eds. Polynomial Approximation: An Alternative to Windowing in Fourier Analysis; Personal Communication. **2011**.
33. Press, W. H.; Teukolsky, S. A.; Vetterling, W. T.; Flannery, B. P. Numerical Recipes in C: The Art of Scientific Computing, 2nd ed.; Cambridge University Press: Cambridge, **1992**.
34. Doppelmayer, N. T. Untersuchung eines Regelkonzepts zum automatischen Füllausgleich bei Mehrkavitäten-Spritzgießwerkzeugen; Bachelor Thesis, Leoben, **2012**.
35. Haase, S. Spectral and Statistical Methods for Vibration Analysis in Steel Rolling; PhD Thesis, Leoben, **2002**.
36. Johannaber, F.; Michaeli, W. Handbuch Spritzgiessen, 2nd ed.; Hanser: München, **2004**.
37. Montgomery, D. C. Design and Analysis of Experiments, 8th ed.; Wiley: Hoboken, NJ, **2013**.